A Switchable Biomimetic Antenna Array

Ines Dorsch, Dominik Schwarz, *Graduate Student Member, IEEE*, and Christian Waldschmidt, *Senior Member, IEEE*

***Abstract*—Biomimetic antenna arrays inspired by the fly *Ormia ochracea* showed a promising improvement of the angle estimation capabilities of radar sensors. So far, there is usually a loss of output power associated with this improvement decreasing the detectability of weak radar targets. In this letter, an electronically switchable two-element biomimetic antenna array is presented for the first time. This array provides the possibility to switch between a biomimetic antenna mode with enhanced phase sensitivity and a conventional antenna mode with a better signal-to-noise ratio. Circuit requirements are discussed, the design process is described, and a realization in the 77 GHz range using p-i-n diodes as switching elements is presented. Radar measurements verify the concept. By switching, the phase sensitivity of the realized array can be enhanced by a factor of three with a relative power loss of maximum 14 dB.**

***Index Terms*—Biologically inspired antennas, biomimetic antenna arrays (BMAAs), direction-of-arrival estimation, millimeter-wave antenna arrays, switched circuits.**

I. Introduction

IT IS a major goal of current radar research to improve radar sensors in their angular performance. Fields where this is of particular importance are advanced driver assistance systems and ultimately autonomous driving [1]. Most efforts take place in the digital domain as the relation between array aperture size and angular resolution sets physical limitations [2]. The so-called biomimetic antenna arrays (BMAAs) use coupling networks inspired by the coupled ears of the fly *Ormia ochracea* [3] and show an enhanced phase sensitivity compared to conventional antenna arrays using the same physical aperture. Consequently, both angle estimation accuracy [4] and, in the case of biomimetic multichannel arrays, angular resolution can be improved [5]. The increased phase sensitivity is accompanied by a reduction of output power, which is the downside of BMAAs and is desired to be avoided.

BMAAs realized to date can be divided into two groups and models. First, there are BMAAs in the lower ultrahigh-frequency band and at cm wavelengths, whose designs depend on mutual coupling of the antenna elements [6]–[8]. Second, there are BMAAs at mm wavelengths, where the biomimetic coupling does not depend on antenna mutual coupling and is realized by precisely designed transmission line transformers connecting the antenna elements [9]–[11].

Masoumi *et al.* [12] presented a BMAA, which strives to achieve phase enhancement with maximum power extraction. However, this approach is not applicable using the more general model of [9]. All BMAAs not depending on antenna mutual coupling showed an inevitable output power loss, whose magnitude depends on the increase of phase sensitivity. In [13], an iterative array design process is used to integrate a varactor in a BMAA. Again, the model relying on mutual coupling is considered, and the design goal differs from this letter as they aim to enlarge the operating bandwidth to 580–700 MHz. Unfortunately, no realization is depicted.

In general, the need of mutual coupling limits the maximum antenna spacing and potential realizations of the antenna elements. Thus, it is advantageous to implement the biomimetic coupling independently of mutual coupling.

This letter presents a switchable BMAA, which does not rely on mutual coupling. This array offers an alternative concerning the fundamental tradeoff between phase sensitivity and signal-to-noise ratio (SNR). p-i-n diodes are incorporated in the biomimetic coupling network (BMC). The resulting array can switch between a biomimetic mode and a conventional array mode. Section II covers BMAA fundamentals. Section III describes the array concept and design. Section IV presents a realized two-element array at 76.5 GHz. Section V presents the measurement setup and results verifying the concept. Section VI concludes this letter.

II. BMAA Fundamentals

The conventional phase difference between two antenna elements is $\phi_{\text{in}} = kd\sin\theta$, where $k = 2\pi/\lambda$ is the free-space wavenumber depending on the wavelength λ, d is the antenna spacing, and θ is the incidence angle of a point target in the far field of the array; see the circuit inset of Fig. 1(a). When incorporating a BMC between the two antennas, the signals at the two output ports (u_1 and u_2) differ from the input signals in amplitude and phase. An example for the biomimetic output phase difference $\phi_{\text{bio}} = \angle u_2 - \angle u_1$ is depicted in Fig. 1(a). The course of ϕ_{bio} is significantly steeper around boresight (BS) ($\theta = 0°$), indicating a much higher phase sensitivity, expressed by the angle-dependent phase gain (similar to [10])

$$\eta_\theta(\theta) = \frac{d\phi_{\text{bio}}(\theta)}{d\theta} \Big/ \frac{d\phi_{\text{in}}(\theta)}{d\theta}. \tag{1}$$

Manuscript received August 24, 2021; accepted September 10, 2021. Date of publication September 20, 2021; date of current version December 20, 2021. This work was supported in part by the Ministry for Science, Research, and Arts Baden-Württemberg within the project ZAFH MikroSens and in part by the German Research Foundation (DFG) under Grant WA 3506/6-2. *(Corresponding author: Ines Dorsch.)*

The authors are with the Institute of Microwave Engineering, Ulm University, 89081 Ulm, Germany (e-mail: ines.dorsch@uni-ulm.de; dominik-1.schwarz@uni-ulm.de; christian.waldschmidt@uni-ulm.de).

Digital Object Identifier 10.1109/LAWP.2021.3113562

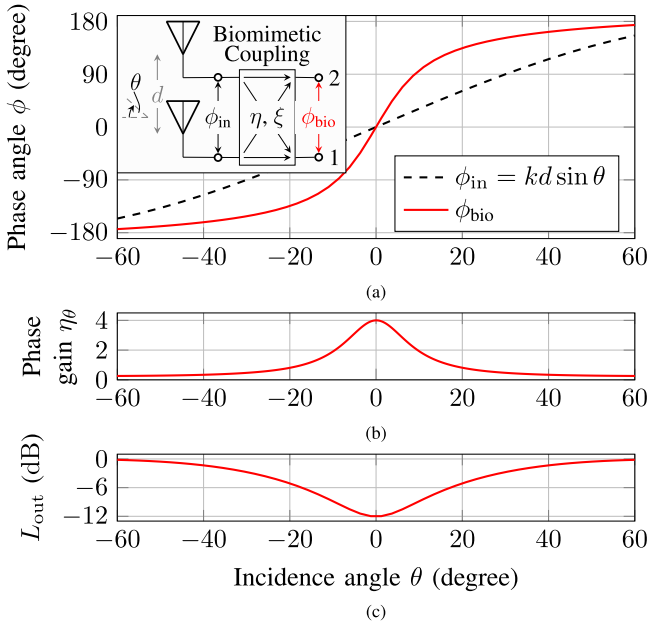

Fig. 1. Exemplary BMAA characteristics for an array with $d = \lambda/2$, $\eta = 4$, and $\xi = 0$ (cf. [11]). (a) ϕ_{bio} compared to the conventional phase progression $kd\sin\theta$, (b) the corresponding η_θ, and (c) L_{out} (equivalent for both ports).

η_θ is 1 for a conventional array for all incidence angles θ. $\eta_\theta > 1$ corresponds to incidence angles with a higher sensitivity compared to a conventional array [see Fig. 1(b)]. If a BMAA has its maximum phase gain off-boresight (off-BS), then η_θ has two maxima lying symmetrically around BS (off-BS characteristic): $\max(\eta_\theta) = \eta_\theta(|\theta_{\max}|)$, $|\theta_{\max}| > 0°$. Three parameters determine the BMAA behavior: the BS phase gain $\eta = \eta_\theta(\theta = 0°)$, the off-BS factor ξ [14], and the antenna spacing d. The influence of the BMC on the amplitude is expressed by the normalized output power [11], [15]

$$L_{\text{out}} = \frac{P_{\text{out,BMAA}}}{P_{\text{out,conv. array}}}. \tag{2}$$

The output power of a BMAA is lower than of a conventional array without BMCs, so $L_{\text{out}} < 1$ applies; cf. Fig. 1(c).

III. Switchable Antenna Concept

In this section, both the concept and the design process for a switchable BMAA are presented. This array has a biomimetic switching state with enhanced phase sensitivity (BIO ON state) and a second state with less phase gain but avoiding the output power loss of the biomimetic coupling (BIO OFF state).

A. Array Behavior

To develop an understanding of what specifications the BMC has to fulfill for the desired task, we now consider the circuit representation depicted in the inset of Fig. 2 instead of the model circuit in Fig. 1(a). The antennas are modeled by an ideal current source and their self-admittance Y_{11}. The BMC in between the two antennas is described by a reciprocal two-port S-parameter matrix $\boldsymbol{S}_{\text{BMC}}$. The antenna elements were chosen

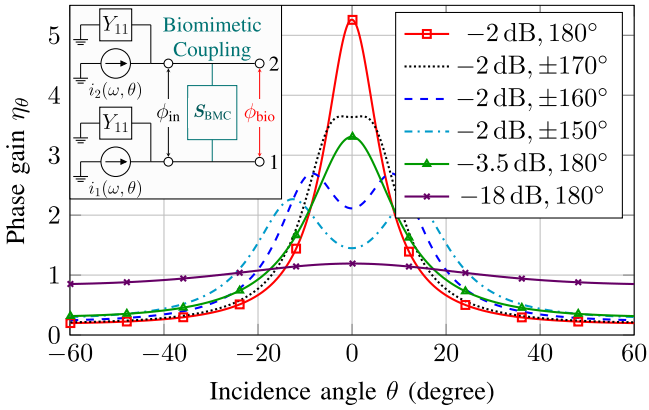

Fig. 2. η_θ for a variation of $S_{\text{BMC},21}$ for $d = \lambda/2$ and a fixed reflection coefficient of $S_{\text{BMC},11} = (-50\text{ dB}, 0°)$. Both transmission magnitude (solid lines) and phase (dashed/dotted lines) influence the phase gain of the BMAA. All curves are symmetrical to BS.

TABLE I
Ideal BMC Values for a Switchable BMAA With Maximum Phase Gain at BS

state	$S_{\text{BMC},21}$		$S_{\text{BMC},11}$	
	$\lvert\cdot\rvert$	$\angle(\cdot)$	$\lvert\cdot\rvert$	$\angle(\cdot)$
BIO ON	high	180°	low	0°
BIO OFF	low	arbitrary	high	0°

identical to the antenna elements in [9] and [10]. The antenna input admittance values of $Y_{11} = 17.48\text{ mS} + \text{j}0.24\text{ mS}$ and $Y_{12} = 2.12\text{ mS} + \text{j}4.41\text{ mS}$ are extracted from full-wave simulations. As $\text{Re}(Y_{12})$ is one order of magnitude smaller than $\text{Re}(Y_{11})$, we neglect the cross-admittance being consistent with the admittance values and circuit simulation of [10]. Fig. 2 shows how η_θ changes when the transmission coefficient $S_{\text{BMC},21}$ is varied. Reflections are neglected ($|S_{\text{BMC},11}| = -50$ dB). For $S_{\text{BMC},21} = (-2\text{ dB}, 180°)$, a BMAA behavior is clearly visible. When introducing a higher attenuation while keeping the transmission phase at 180°, the maximum phase gain is reduced. Thus, the phase gain converges to 1 for all angles and small magnitude values of $S_{\text{BMC},21}$. This corresponds to the conventional array without biomimetic coupling or the BIO OFF state.

If the maximum phase gain is desired to occur at BS, the transmission phase of 180° has to be met quite precisely, as deviations in $\angle S_{\text{BMC},21}$ lead to an off-BS behavior (see Fig. 2). The reflection coefficient $S_{\text{BMC},11}$ also has an influence, if its magnitude is not negligible. Higher reflections lead to less power passing through the BMC and less phase gain results. The reflection phase also impacts the biomimetic characteristic (BIO ON state) even though its deviations from $\angle S_{\text{BMC},11} = 0°$ are less critical compared to the transmission phase. Especially, for the BIO OFF state, an open-circuit and, thus, an unaltered conventional antenna operation is desired. This corresponds to a phase of $\angle S_{\text{BMC},11} = 0°$.

The specifications needed for a switchable BMAA with maximum phase sensitivity at BS are listed in Table I. Generally, the output signal at one port is a superposition of the signal from

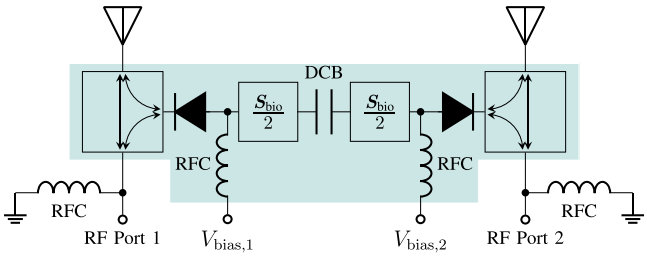

Fig. 3. Schematic of the switchable BMAA. The array is built up symmetrically. The two bias paths are separated by a DCB, whereas the RF path is isolated from the DC path by RFCs. The components influencing the BMC are highlighted.

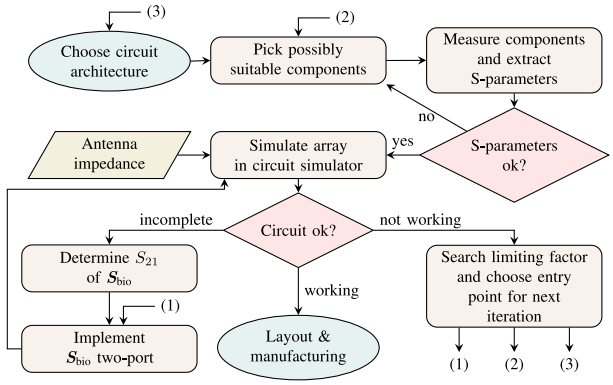

Fig. 4. Flowchart for the switchable BMAA design process.

its antenna, the reflected signals, and the signal received by the other antenna that passes through the BMC.

B. Array Design Process

First, a suitable circuit architecture has to be chosen. The circuit considered in this letter is shown in Fig. 3. p-i-n diodes are used as switching elements. The architecture in Fig. 3 is symmetrical, and the signals at both RF ports are identically influenced by the BMC. The p-i-n diodes are connected in the serial mode and are independently biased with the voltages $V_{\mathrm{bias},1}$ and $V_{\mathrm{bias},2}$. The bias paths are separated by a DC block (DCB) capacitor. The RF signal is blocked from the bias paths by RF chokes (RFCs). T-junctions connect the antennas, the BMC, and the output ports. They influence the S-parameters of the coupling path and are, therefore, also modeled. At least, one additional component has to be introduced in the coupling path to adjust the S-parameters of the BMC to the values wanted for a specific BMAA behavior. The component ensuring the right overall BMC S-parameters is expressed as $\boldsymbol{S}_{\mathrm{bio}}$ and is distributed on both sides of the DCB to maintain symmetry.

The array is switched to its conventional mode (BIO OFF state) when the diodes are biased to be nonconducting. For high reflection values of the nonconducting diodes, ideally, no output power is lost due to the biomimetic coupling. The output signals are mainly influenced by the reflection phase of the diodes. When the diodes are conducting, then the antennas are biomimetically coupled (BIO ON state), and the BMAA behavior is determined by the BMC component chain.

The workflow to develop such arrays is depicted in Fig. 4. After deciding on a circuit architecture, the individual components have to be selected and characterized by measurements. The measured S-parameters of all components are checked for their suitability. Particularly relevant is the difference in the transmission magnitude of the switching component between ON and OFF states. For a better evaluation, the circuit is built up in an RF circuit simulation tool using the measured S-parameters of the components. Next, the transmission values of $S_{\mathrm{bio},21}$ have to be determined so that the crucial transmission coefficient requirements of the BMC are met. While the two ports characterized by $\boldsymbol{S}_{\mathrm{bio}}$ can be discrete, an implementation in form of a distributed transmission line component was chosen (determined using full-wave simulations). If the complete simulated circuit fulfills its task for both switching states, it can be manufactured.

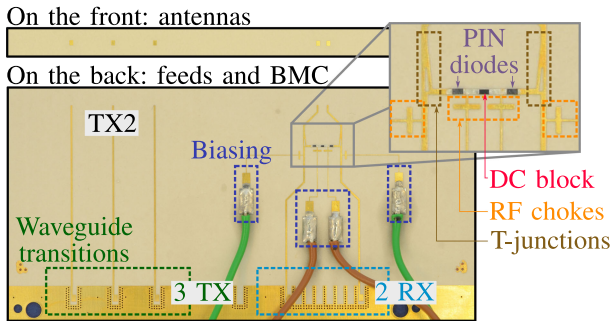

Fig. 5. Photography of the realized antenna board including the switchable two-element BMAA being the receive (RX) array. Only transmit (TX) antenna 2 is considered.

If the desired behavior is not met, adaptions have to be made. So, first, the $\boldsymbol{S}_{\mathrm{bio}}$ component, then the discrete components, and, if necessary, the circuit architecture are analyzed and revised, or replaced in that order.

It is apparent that the design procedure can take multiple iterations depending on the chosen circuit architecture, circuit components, and the feasible $\boldsymbol{S}_{\mathrm{bio}}$ values. In order to obtain a considerable phase gain in the BIO ON state, components with low attenuation must be available at the operational frequency (discrete components) or realizable (distributed components), respectively.

IV. Realization

The realized antenna array is depicted in Fig. 5. The antenna board is built up by a stack of two 127 μm thick Rogers RO3003 layers fused with an RO3001 bonding film. Aperture-coupled patch antennas as in [9] are used, separating the radiating elements and the feeding network spatially. The RFC is realized by two parallel open-ended stubs and a quarter-wave transformer [16]. The T-junction used in this letter was optimized to have little influence on the phase of the transmission coefficient of the BMC in [10]. The DCB is a thin-film silicon capacitor from Murata. The p-i-n diodes are model MA4AGFCP910 from Macom. In this letter, the diodes are used in an interchanged way. The measurements at 76.5 GHz showed that the diodes are less conducting when forward-biased. This behavior can be attributed to the package parasitics and circuit setup. Thus, the

TABLE II
BMC VALUES FOR THE REALIZED SWITCHABLE BMAA

state	$S_{\mathrm{BMC},21}$	$S_{\mathrm{BMC},11}$	$\max(\eta_\theta)$	$\min(L_{\mathrm{out}})$
BIO ON	$-2.19\,\mathrm{dB}$	$-7.33\,\mathrm{dB}$	4.1	$-14.9\,\mathrm{dB}$
	$-199°$	$-103°$	$@\theta = 0°$	
BIO OFF	$-7.04\,\mathrm{dB}$	$-5.20\,\mathrm{dB}$	1.1	$-2.9\,\mathrm{dB}$
	$106°$	$-25°$	$@\theta = 0°$	

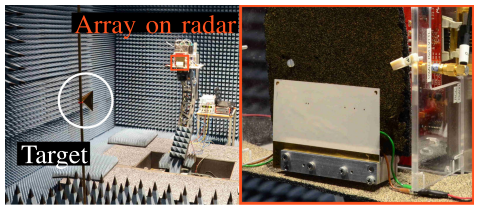

Fig. 6. Measurement setup in an anechoic chamber and a close-up of the antenna board mounted on the radar.

BIO OFF state corresponds to forward-biased diodes and the BIO ON state is set for reverse-biased (RB), respectively.

The equivalent S-parameters of the components forming the coupling path met the desired transmission magnitude, so the two ports specified by $\boldsymbol{S}_{\mathrm{bio}}$ do not have to introduce additional attenuation. The two $\boldsymbol{S}_{\mathrm{bio}}/2$ blocks in Fig. 3 are, thus, only needed to adjust the transmission phase and were realized by transmission lines of 610 μm length.

The resulting simulated S-parameters of the realized coupling network (without the T-junction) are noted in Table II. Also, the resulting simulated BMAA behavior in form of the maximum phase gain and minimum L_{out} is listed. Enabling the biomimetic coupling results in a significant phase gain. The simulated loss of output power in the BIO OFF state is not larger than 2.9 dB.

V. MEASUREMENTS

To prove the functionality of the proposed antenna circuit, radar measurements were conducted in an anechoic chamber. A chirp-sequence modulated radar with a carrier frequency of 76.5 and 2 GHz bandwidth [17] was mounted on a turntable. Radar measurements using a single target were performed for incidence angles of $-60° \leq \theta \leq 60°$ (see Fig. 6). Conventional range-Doppler processing was performed, and the steering vectors were extracted from the target bin for every incidence angle [18], [19]. The results are shown for four different bias points ($V_{\mathrm{bias},1} = V_{\mathrm{bias},2}$): $V_{\mathrm{bias},1} = 0\,\mathrm{V}, 1.2\,\mathrm{V}$ (forward current $I_{\mathrm{F}} \approx 0.7\,\mathrm{mA}$), $\approx 1.4\,\mathrm{V}$ ($I_{\mathrm{F}} = 10\,\mathrm{mA}$), and $-5\,\mathrm{V}$. Furthermore, the same measurements were carried out for a conventional array, which is identical except that the BMC and biasing structures are not included. Fig. 7 clearly shows two different phase progression behaviors. When unbiased or reverse-biased, an increased phase sensitivity around BS corresponding to a BS phase gain of $\eta = 4.5$ can be recognized. For forward bias (FB), the array behaves exactly like the conventional array using the same antenna elements and spacing. Due to a nonperfect decoupling of the antenna elements, a minor phase gain of $\eta = 1.5$ is present for the conventional array.

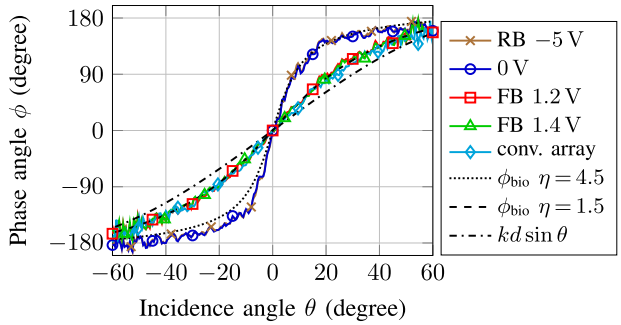

Fig. 7. Measured ϕ_{bio} for four bias points. For 0 V and RB, the array is switched to the BIO ON state. The array shows the same phase progression when forward-biased as when a conventional array without BMC is used.

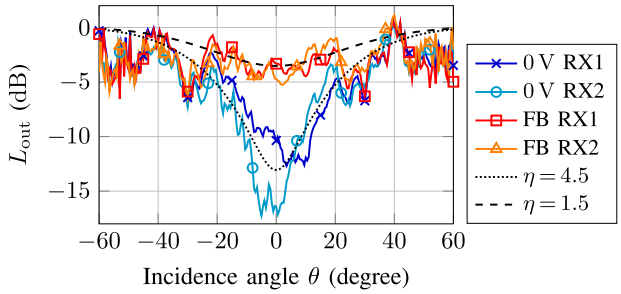

Fig. 8. Measured L_{out} of the two BMAA ports for 0 and 1.2 V FB. When forward-biased, the array does not show the typical angle-dependent power loss around BS. The theoretical curves for $\eta = 1.5$ and $\eta = 4.5$ (both $\xi = 0$) are identical for both ports.

The course of L_{out} shows the desired behavior (see Fig. 8). For clarity, only one bias point per switching state is depicted. Similar to the phase gain, the measured L_{out} is insensitive to bias variations within one switching state. In the BIO ON state, the measured L_{out} curves match the theoretical curve very well and the minimum measured L_{out} is $-17\mathrm{dB}$. In the BIO OFF state, an angle-independent L_{out} level can be measured, proving the proper operation of this switching state. The characteristic output power loss around BS is avoided. Conceivable reasons for the L_{out} level of about -3 dB in the BIO OFF state are both nonideal amplitude and phase of the reflection coefficient of the diodes, as well as deviations in the printed circuit board quality between the BMAA antenna board and the conventional antenna board.

VI. CONCLUSION

In this letter, the concept and the design process of a switchable BMAA are presented. This array addresses the typical tradeoff of comparable BMAAs between a better angular sensitivity and a reduced output power. Radar measurements of a realization at 76.5 GHz verified design and simulations very well. The presented realization can either achieve a phase gain of $\eta = 4.5$ with a maximum power loss of 17 dB or a phase behavior identical to a conventional array with only around 3 dB power loss for all incidence angles. The switchable biomimetic array offers an adaptivity depending on the target parameters. In the future, target parameters can be determined in a two-step process. First, the target is detected with better SNR; then, the direction-of-arrival can be estimated with better accuracy.

REFERENCES

[1] C. Waldschmidt, J. Hasch, and W. Menzel, "Automotive radar—From first efforts to future systems," *IEEE J. Microw.*, vol. 1, no. 1, pp. 135–148, Jan. 2021.

[2] I. Bilik, O. Longman, S. Villeval, and J. Tabrikian, "The rise of radar for autonomous vehicles: Signal processing solutions and future research directions," *IEEE Signal Process. Mag.*, vol. 36, no. 5, pp. 20–31, Sep. 2019.

[3] R. N. Miles, D. Robert, and R. R. Hoy, "Mechanically coupled ears for directional hearing in the parasitoid fly Ormia ochracea," *J. Acoust. Soc. Amer.*, vol. 98, no. 6, pp. 3059–3070, Dec. 1995.

[4] P. Grüner, T. Chaloun, and C. Waldschmidt, "Enhanced angle estimation accuracy of ultra compact radars inspired by a biomimetic approach," in *Proc. IEEE MTT-S Int. Microw. Symp.*, Jun. 2017, pp. 1425–1428.

[5] I. Dorsch, P. Grüner, M. Klose, D. Schmucker, and C. Waldschmidt, "Performance evaluation and optimization of MIMO radars using biomimetic antenna arrays," *IEEE Trans. Microw. Theory Techn.*, to be published, doi: 10.1109/TMTT.2021.3103579.

[6] A. R. Masoumi, Y. Yusuf, and N. Behdad, "Biomimetic antenna arrays based on the directional hearing mechanism of the parasitoid fly Ormia ochracea," *IEEE Trans. Antennas Propag.*, vol. 61, no. 5, pp. 2500–2510, May 2013.

[7] P. Grüner, T. Chaloun, and C. Waldschmidt, "Towards a mm-wave planar biomimetic antenna array with enhanced phase sensitivity," in *Proc. 10th Eur. Conf. Antennas Propag.*, Apr. 2016, pp. 1–5.

[8] Y. Zang, H. Luyen, H. R. Bahrami, and N. Behdad, "An analytic synthesis method for two-element biomimetic antenna arrays," *IEEE Trans. Antennas Propag.*, vol. 68, no. 4, pp. 2797–2809, Apr. 2020.

[9] P. Grüner, T. Chaloun, and C. Waldschmidt, "A generalized model for two-element biomimetic antenna arrays," *IEEE Trans. Antennas Propag.*, vol. 67, no. 3, pp. 1630–1639, Mar. 2019.

[10] P. Grüner, I. Dorsch, and C. Waldschmidt, "N-element biomimetic antenna arrays," *IEEE Trans. Antennas Propag.*, vol. 69, no. 7, pp. 3899–3912, Jul. 2021.

[11] P. Grüner, M. Geiger, and C. Waldschmidt, "Ultracompact monostatic MIMO radar with nonredundant aperture," *IEEE Trans. Microw. Theory Techn.*, vol. 68, no. 11, pp. 4805–4813, Nov. 2020.

[12] A. R. Masoumi, K. Ghaemi, and N. Behdad, "A two-element biomimetic antenna array with enhanced angular resolution and optimized power extraction," *IEEE Trans. Antennas Propag.*, vol. 63, no. 3, pp. 1059–1066, Mar. 2015.

[13] M. R. Nikkhah, K. Ghaemi, and N. Behdad, "An electronically tunable biomimetic antenna array," *IEEE Trans. Antennas Propag.*, vol. 66, no. 3, pp. 1248–1257, Mar. 2018.

[14] P. Grüner, S. Nguyen, T. Chaloun, and C. Waldschmidt, "Enhancing angle estimation for off-boresight targets using biomimetic antenna arrays," in *Proc. 48th Eur. Microw. Conf.*, Sep. 2018, pp. 1377–1380.

[15] A. R. Masoumi and N. Behdad, "An improved architecture for two-element biomimetic antenna arrays," *IEEE Trans. Antennas Propag.*, vol. 61, no. 12, pp. 6224–6228, Dec. 2013.

[16] I. Flammia, T. Kleinfeld, M. Frei, A. Utreras-Rivera, and A. Stöhr, "71–76 GHz grounded-coplanar-waveguide-to-rectangular-waveguide transition with integrated planar bias tee for quasi-hermetic radio-over-fiber wireless transmitter," in *Proc. 7th Eur. Microw. Integr. Circuit Conf.*, Oct. 2012, pp. 512–515.

[17] P. Hügler, F. Roos, M. Schartel, M. Geiger, and C. Waldschmidt, "Radar taking off: New capabilities for UAVs," *IEEE Microw. Mag.*, vol. 19, no. 7, pp. 43–53, Nov./Dec. 2018.

[18] V. Winkler, "Range Doppler detection for automotive FMCW radars," in *Proc. Eur. Radar Conf.*, Oct. 2007, pp. 166–169.

[19] C. Vasanelli *et al.*, "Calibration and direction-of-arrival estimation of millimeter-wave radars: A practical introduction," *IEEE Antennas Propag. Mag.*, vol. 62, no. 6, pp. 34–45, Dec. 2020.